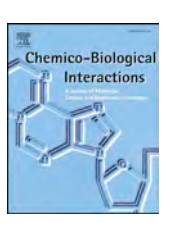
FISEVIER

Contents lists available at ScienceDirect

Chemico-Biological Interactions

journal homepage: www.elsevier.com/locate/chembioint



Development of a magnetic nano-graphene oxide carrier for improved glioma-targeted drug delivery and imaging: In vitro and in vivo evaluations



Sakine Shirvalilou^a, Samideh Khoei^{a,b,*}, Sepideh Khoee^c, Nida Jamali Raoufi^d, Mohammad Reza Karimi^c, Ali Shakeri-Zadeh^a

- ^a Department of Medical Physics, School of Medicine, Iran University of Medical Sciences, Tehran, Iran
- ^b Razi Drug Research Centre, Iran University of Medical Sciences, Tehran, Iran
- ^c Department of Polymer Chemistry, School of Sciences, University of Tehran, Tehran, Iran
- ^d Department of Physiology, School of Medicine, Iran University of Medical Sciences, Tehran, Iran

ARTICLE INFO

Keywords: Superparamagnetic iron oxide Glioma Magnetic targeting 5-lodo-2'-deoxyuridine Nano-graphene oxide

ABSTRACT

To overcome the obstacles inflicted by the BBB in Glioblastoma multiforme (GBM) we investigated the use of Multifunctional nanoparticles that designed with a Nano-graphene oxide (NGO) sheet functionalized with magnetic poly (lactic-co-glycolic acid) (PLGA) and was used for glioma targeting delivery of radiosensitizing 5iodo-2-deoxyuridine (IUdR). In vitro biocompatibility of nanocomposite has been studied by the MTT assay. In vivo efficacy of magnetic targeting on the amount and selectivity of magnetic nanoparticles accumulation in glioma-bearing rats under an external magnetic field (EMF) density of 0.5 T was easily monitored with MRI. IUdR-loaded magnetic NGO/PLGA with a diameter of 71.8 nm, a zeta potential of -33.07 ± 0.07 mV, and a drug loading content of 3.04 ± 0.46% presented superior superparamagnetic properties with a saturation magnetization (Ms) of 15.98 emu/g. Furthermore, Prussian blue staining showed effective magnetic targeting, leading to remarkably improved tumor inhibitory efficiency of IUdR. The tumor volume of rats after treatment with IUdR/NGO/SPION/PLGA + MF was decreased significantly compared to the rats treated with buffer saline, IUdR and SPION/IUdR/NGO/PLGA. Most importantly, our data demonstrate that IUdR/NGO/SPION/PLGA at the present magnetic field prolongs the median survival time of animals bearing gliomas (38 days, p < 0.01). Nanoparticles also had high thermal sensitivities under the alternating magnetic field. In conclusion, we developed magnetic IUdR/NGO/PLGA, which not only achieved to high accumulation at the targeted tumor site by magnetic targeting but also indicated significantly enhanced therapeutic efficiency and toxicity for glioma both in vitro and in vivo. This innovation increases the possibility of improving clinical efficiency of IUdR as a radiosensitizer, or lowering the total drug dose to decrease systemic toxicity.

1. Introduction

Glioblastoma is the most common malignant primary brain tumor, with invasive nature and high proliferation rate, characterized by diffusely infiltrate neighboring brain tissue and tremendous biological heterogeneity [1,2]. Despite the development of conventional therapies that include invasive surgery, radiation therapy and chemotherapy, because of high recurrence rates, the prognosis remains very poor [3]. In most cases, it is impossible to completely eradicate malignant glioma by surgery even when combined with radiotherapy and chemotherapy due to major challenges in tumor such as infiltration rate, resistant cancer stem cells, drug delivery through the BBB and the difficulty

retaining a therapeutically drug concentration at the tumor lesions [4,5]. BBB is formed by the endothelial layer with tight junctions that prevents effective targeting of diagnostic and therapeutic agents to tumor areas [6]. Most of the current anticancer agents such as radiosensitizers have short half-life time, poor hydrolytic stability and suffer from inefficiency to penetrate the BBB. Over the past decade, nanotechnology has represented an innovative approach as nanoparticle-based drug delivery systems to overcome the BBB transport [7]. Multifunctional nanoparticles (NPs) are powerful tools for current clinical diagnostics and therapeutic procedures. Nanoparticles could protect the drugs from metabolic degradation, increase circulation lifetime and decrease the rate of clearance from the blood, increase tumor drug

E-mail addresses: khoei.s@iums.ac.ir, skhoei@gmail.com (S. Khoei).

^{*}Corresponding author. Razi Drug Research Centre, Department of Medical Physics, School of Medicine, Iran University of Medical Sciences, P.O.Box: 1449614525, Tehran, Iran.

delivery, control release and decrease unwanted side effects [8,9]. Actually, Poly (lactic-co-glycolic acid) (PLGA) due to their adjustable characteristics such as biocompatibility, biodegradability and nontoxicity are considered as useful nanocarriers for the delivery of drugs and agents [10,11].

Graphene is a two-dimensional sp² carbon networking nanomaterial that offers excellent potential in the drug delivery field because of its hexagonal carbon ring structure which allowed hydrophobic interactions, electrostatic interaction and π - π stacking with anticancer drugs with aromatic ring structures [12,13]. Graphene oxide (GO) sheets are important derivatives of graphene that have high drug-loading efficiency (both sides of a graphene oxide sheets can be used for drug loading), excellent biocompatibility and unclear toxicity. GO sheets modified with biocompatible polymers such as PLGA showed increased stability in physiological solutions for delivery of aromatic anticancer drugs and also did not indicate any significant acute toxicity on intravenous (i.v.) injection into mice [14,15]. Halogenated pyrimidines such as, 5-iodo-2-deoxyuridine are an important family of radiosensitizers [16]. Enhanced cell killing after radiotherapy is a desirable effect observed in cells treated with IUdR, which is due to the Auger emissions from the high-Z iodine [17]. It is a halogenated thymidine analogue, which is incorporated into DNA instead of thymine for phosphorylation, during the S phase of mitotic cells [18]. Due to the differential effects of IUdR, glioma tumor cells gradually become more sensitive to radiation damage. Though, IUdR is widely used to improve radiation efficacy but it has a short metabolic half-life in the circulation and can hardly cross through blood-brain barrier, which limits its clinical utility on glioma malignant [19]. In order to overcome these problems, we commonly use the Superparamagnetic iron oxide nanoparticles (SPIONs) [20,21].

SPIONs have attracted attention in the past decades due to their unique capability in noninvasive brain tumors diagnostics and therapeutics in one multifunctional platform. Since nanoparticles pass the BBB, they could be useful in the development of novel therapeutic procedures [5,22]. SPIONs can be used simultaneously for drug delivery and as magnetic resonance imaging (MRI) contrast agents, because they can be properly modified to carry anticancer agents, be magnetically guided to the targeted areas and retained at tumor areas by applying an external magnetic field as a local. Since SPIONs are powerful enhancers of proton spin–spin (T2/T2*) relaxation, MRI imaging is a suitable method for non-invasive real-time detection of such NPs, thus improving the differentiation of malignancy from normal brain tissue [6,23].

In the present study, we synthesized and tested a multifunctional nanoparticle as magnetic graphene oxide-based nanocarrier (NGO/SPION/PLGA) structure incorporating therapeutic agent (IUdR). These multifunctional magnetic nanoparticles were designed to not only target gliomas by applying external magnetic fields (magnetic Nd–Fe–B), induce BBB-opening and therapeutic drug delivery, but also serve as MRI contrast agent for real-time monitoring of nanoparticles inside tumor sites. Finally, the antitumor efficiency and safety of the IUdR-loaded multifunctional nanoparticles for loading and glioma magnetic targeting delivery of anticancer agent IUdR (IUdR/NGO/SPION/PLGA) was evaluated using by C6 glioma cell line and glioblastoma-bearing rats via systemic administration.

2. Material and methods

2.1. Materials

Cell culture medium (Ham's F-12) and Penicillin-Streptomycin were purchased from Atocel (Austria). Fetal bovine serum (FBS) was obtained from Biowest (France). 3-(4,5- dimethylthiazol-2-yl)-2,5-diphenyltetrazolium bromide (MTT), Iron (III) chloride hexahydrate (FeCl₃.6H₂O) pure granulated, 99%, Iron (II) chloride tetrahydrate (FeCl₂.4H₂O) 99%, Dimethyl sulfoxide (DMSO), Trypsin-EDTA, Tween

60, Span series, Graphite and potassium permanganate (KMnO $_4$) were purchased from Sigma–Aldrich. PLGA (MW = 25,000 Da, LA/GA = 50/50) was obtained from PolySciTech (USA). Hydrochloric acid (37%) and Nuclear fast red purchased from Merck.

2.2. Cell line and monolayer culture

The C6 rat glioma cell line was purchased from the Cell Bank of the Pasteur Institute of Iran. The C6 cells were cultured at $37\,^{\circ}$ C in a humidified environment with 5% CO₂ within Ham's F-12 medium supplemented by 10% heat-inactivated fetal bovine serum, penicillin ($100\,$ U/mL), and streptomycin ($100\,$ mg/mL).

2.3. Synthesis of magnetic NGO/PLGA nanoparticles

2.3.1. Synthesis of magnetite nanoparticles

Chemical co-precipitation method was used for the synthesis of superparamagnetic iron oxide nanoparticles according to a previously reported method [24]. Briefly, a mixture of FeCl $_3$.6H $_2$ O (2.4 g) and FeCl $_2$.4H $_2$ O (0.8 g) was dissolved in deionized water in a three-necked round bottom flask and stirred using mechanical stirrer at 70 °C and argon atmosphere. During stirring, 10 ml of ammonia solution (25%) was added dropwise. After 2 h of stirring, the magnetite nanoparticles were magnetically separated. For purification, the nanoparticles were washed by deionized water 3–4 times and two times with ethanol and then dried in vacuum at 45 °C.

2.3.2. Synthesis of nanographene oxide (NGO)

Nanographene oxide was synthesized from graphite powder (purity. 99.99%) using improved hummers method as reported [25]. In brief, graphite (1.0 g) was mixed with $\rm H_2SO_4$: $\rm H_3PO_4$ (180:20 ml) under constant stirring. After a steady addition of KMnO₄ (6.0 g), the mixture was let to stir for 3 days in 50 °C. The solution was poured into ice water and then $\rm H_2O_2$ solution was added dropwise till the color of the suspension changed to bright yellow. The obtained graphite oxide solution was centrifuged repeatedly and washed with deionized water and 10% of HCl aqueous solution, three times to adjust the pH of the solution to 4–5. During the second washing process the graphite oxide experienced exfoliation, which resulted in a NGO gel formation.

2.3.3. Nanoparticle preparation

IUdR-loaded magnetic (NGO/PLGA) nanoparticles were synthesized according to the procedure of Khoee et al. with some modifications [26]. In summary, magnetic nanoparticles were prepared using a modified O1/W1/O2/W2 multiple emulsion solvent evaporation method. Glycerin was used as a surfactant to stabilize the dispersed phase. First, 30 mg of magnetite nanoparticles (9.6 ± 0.41 nm in diameter) was dispersed in dichloromethane (DCM) (0.5 ml) to prepare a primary organic phase (O1) using an ultrasonic bath. Then, the inner aqueous solution was prepared, at first 5 mg of graphene oxide was dispersed in double distilled water, and then, Tween60 (15 mg) was dissolved as a surfactant into the graphene oxide solution. IUDR (10 mg), as an anti-cancer drug, was dissolved in DMSO (0.2 ml), and then, it was added into the prepared graphene oxide solution (W1). The magnetic dispersion (O1) was emulsified in the inner aqueous solution (W1) via ultrasonication using the sonicator probe with an output of 50 W for 45 s in an ice-bath to obtain an O1/W1 emulsion (dispersion of magnetite). This primary emulsion was emulsified in an organic solution (O2) of the polymer (50 mg PLGA (50:50) and Span60 (250 mg) in 6 ml of DCM by ultrasonication for 45 s (50 W) in an ice-bath to gain an O1/W1/O2 double emulsion. Next, this double emulsion was immediately poured into 15 ml of W2 aqueous solution, which was made of Tween60 (150 mg) dissolved in 7.5 ml of distilled water and 7.5 ml of glycerin, and the mixture was again ultrasonicated for 30 s. The resulted emulsion (O1/W1/O2/W2) was diluted in 24 ml of aqueous solution composed of distilled water (12 ml) and glycerin (12 ml) under

mechanical stirring, and the DCM was removed by solvent evaporation. The stirring was kept for a period of 4 h at room temperature (25 °C) to allow the evaporation of the organic solvent. The resulting magnetic nanoparticles were cleaned by repeating the centrifugation procedure and re-suspension in distilled water 3–4 times, and then, were collected with a magnet. The most of non-encapsulated drugs remained in the outer aqueous solution, and the remained drugs, loosely adsorbed on the surface of the nanoparticles, were removed by washing with double distilled water. At last, the magnetic nanoparticles freeze-dried using automatic freeze dryer (Tajhizat Sazan Pishtaz, Iran) and stored at 4 °C. Additionally, magnetic nanoparticles (empty nanoparticles) were synthesized in the same way, but without IUdR.

2.4. Characterization of nanoparticles

The morphological examination of IUdR-loaded magnetic nanoparticles (NGO/PLGA) was performed via Transmission electron microscopy (TEM; Zeiss LEO906, Jena, Germany). The hydrodynamic sizes and zeta potentials of the nanoparticles were characterized through a (Brookhaven Instruments, Holtsville, NY, USA). The magnetic properties of the resultant samples were determined by a Vibrating-sample magnetometer (PAR 155; USA).

2.4.1. Drug-loading and encapsulation efficiency

Concentration of IUdR loading on NGO/SPION/PLGA was measured using the absorbance peak from UV/Visible Spectrophotometer (Ultrospec 3000, Pharmacia biotech, USA). First, the samples of (freezedried) nanoparticles were weighed (3 mg) and dissolved in 5 ml of acetone (spectroscopy grade). Next, the insoluble magnetite nanoparticles were removed from the supernatant by magnetic separation and centrifuged at 3000 rpm for 15 min. Finally, the IUdR concentration in the acetone solution was indicated by UV absorption at a wavelength of 288 nm (characteristic absorption band of IUdR), Empty nanoparticles of IUdR were used as a blank test. According to the standard curve, drug loading and encapsulation efficiency of nanoparticles were obtained using Eq. (1) and Eq. (2) respectively:

Drug loading content (%) =
$$\frac{\text{Weight of the drug in nanoparticle}}{\text{Weight of the nanoparticle}} \times 100$$

(1)

$$\label{eq:encapsulation} \text{Encapsulation efficiency (\%) = } \frac{\text{Weight of the drug in nanoparticle}}{\text{Weight of the feeding drug}} \times 100$$

(2)

2.4.2. In vitro drug release

The cumulative release of IUdR from the magnetic nanoparticles was carried out in PBS medium at physiological pH (pH \sim 7.4), using the dialysis tube diffusion method. 5 mg of drug loaded nanoparticles was suspended in 1 mL PBS and the solution was introduced into a preactivated dialysis bag (cutoff molecular weight 12,400 Da). Both ends of the dialysis tube were fixed with clamps and then immersed in 50 mL of PBS as a release medium placed on incubator shaker with constant temperature at 37 °C. At predetermined intervals, 1 ml of external release medium was sampled and replaced with an equal volume of fresh release medium, with the same amount of fresh buffer. The IUdR concentration was obtained based on the absorbance of IUdR at 288 nm by using the standard curve of IUdR in the PBS. Drug release percentage was determined by Eq. (3):

Drug release (%) =
$$C_t/C_{max} \times 100$$
 (3)

Where C_t and C_{max} represent the IUdR concentration at the time t, and the maximum concentration of IUdR that can be released, respectively. Finally, the percentage of released drug from NGO/PLGA magnetic nanoparticles WAS plotted against time. All the release studies were carried out in triplicate.

2.4.3. Alternative magnetic field exposure and thermal sensitivity study

Photothermal properties of the prepared magnetic nanoparticles were assessed with radiofrequency coil where the alternative magnetic field (AMF) strength had reached its maximum value (40 kA/m, 13.56 MHz). For this reason, 20 mg of the nanoparticles were dispersed in the Ham's F-12 medium and added to the flask T-25. Then, the flask was located at center of the RF coil. During the AMF exposure, the temperature increase was monitored using an infrared camera (Testo 875-2i, United Kingdomhttps://www.testo.com/en-UK/parameters/thermal-imaging-cameras/c/parameters_thermal_imager) every 1 min for 10 min.

2.5. In vitro cytotoxicity evaluation

The cytotoxicity of nanoparticles to C6 glioma cells was assessed with the MTT cell viability assay. The cells were seeded into 96-well plates with a density of 5×10^4 cells/well and cultured in 100 µL of Ham's F-12 complete medium in an environmental chamber at 37 °C in 5% CO2 for overnight. Free IUdR, NGO and SPION (uncoated), IUdRloaded NGO/SPION/PLGA, and NGO/SPIONS/PLGA at different concentrations were dissolved in $100\,\mu L$ of serum-free medium, respectively, and then added into each well. The final concentration of IUdR in the medium was maintained in the range of 0-70 mg/mL. Five wells untreated cells were used as controls. After 24 h, the cells were washed twice with PBS then 100 µL of MTT (5 mg/mL in PBS) was added to each well and the plates were incubated at 37 °C for 4 h in the dark. The medium was removed and $100\,\mu\text{L}$ of DMSO was added to dissolve the blue formazan crystals for 15 min. The absorbance was read on an ELISA Reader at 540 nm. The survival percentages were calculated using Eq. (4):

Survival (%) =
$$(A540 \text{ nm} \text{ for the treated cells/}A540 \text{ nm} \text{ for the control cells}) \times 100$$
 (4)

Each assay was carried out in triplicate. Finally, concentration via viability curves were made and the half maximal inhibitory concentration (IC50) values were calculated.

2.6. Experimental animals

Male Wistar rats (200–220 g) were obtained from the Experimental Studies Center of Iran University of Medical Sciences (Tehran, Iran) and maintained under natural light/dark conditions. Animals were allowed free access to standard food and water. The temperature and relative humidity were kept at 25 $^{\circ}$ C and 50%, respectively. All the care and handling of animals were performed according to the guidelines of animal research committee of Iran University of Medical Sciences and were also approved for Ethics in Animal Experiments (No. IR. IUMS.REC 1394, 9221339201).

2.6.1. C6 rat brain tumor model

Rats were anesthetized by intraperitoneal injection of ketamine (75 mg/kg body weight) and xylazine (5 mg/kg). The animals' heads were shaven and eyes lubricated with an ocular lubricant. The rats were immobilized on a stereotactic frame. A small skin incision was made and a 1-mm hole was drilled through the skull positioned 2 mm anterior and 2 mm lateral to bregma on the right-hand side of the head. Approximate 1×10^6 C6 glioma cells/10 μl in serum-free Hams F12 medium using a Hamilton syringe (23 G) were injected into the cortex with a depth of 4-mm and a rate of $2\,\mu L/min$. The needle was left in place for an additional 4 min and then withdrawn slowly. The hole was closed using bone wax and the incision was sutured. Animals were assessed longitudinally by MRI at 14 days' post-cell implantation to select tumors between 70 and 100 mL in volume.

2.7. In vivo magnetic targeting using the modified magnet configuration

Magnetic targeting studies were carried out in C6 glioma tumorbearing rats using intravenous nanoparticle administration under permanent magnetic fields. Animals were placed ventrally on a platform with their head positioned between two blocks neodymium-iron-boron permanent magnet with a magnetic field strength of 1.3 T (NdFeB, $100 \times 50 \times 50$ mm) with the right and left sides of the head each having a distance of 0.5 and 1.5 cm from the corresponding blocks, respectively. Magnetic set up was optimized to achieve sharp gradient of magnetic flux density at the target location. Measurements of magnetic density in the space between the two blocks were performed using a tangential B-probe Teslameter (LEYBOLD, Germany), IUdR-loaded NGO/SPION/PLGA were injected into the tail vein of rats with a dose of 9 mg/kg (contain 2 mg/kg Fe) seventeen days after implantation and retained in the magnetic field for 1 h [27,28]. To evaluate brain-targeting ability of nanoparticles, the rats were imaged with MRI before the administration of nanoparticles and after the magnetic targeting. Following MRI imaging, the rats were sacrificed and the brains were collected.

2.8. Determination of nanoparticle through Prussian blue staining

The accumulation of multifunctional nanoparticles in tumor tissues was evaluated using Prussian blue staining to identify nuclei and iron. Rats were sacrificed 1 h after the injection of nanoparticle and magnetic targeting. The brain tissue samples were fixed immediately in 10% formalin for 48 h at 25 °C. The samples were dehydrated in ethanol, embedded in paraffin, cryosections (4- μm thickness), and stained Prussian blue. Slices were incubated with 10% potassium ferrocyanide and 20% hydrochloric acid for 10 min, washed and counterstaining with Nuclear Fast Red.

2.9. In vivo magnetic resonance imaging (MRI)

All MRI images were acquired on a 3T scanner (MAGNETOM Prisma, Siemens, Germany) equipped with a rat head receive coil. Animals were anesthetized with ketamine (40 mg/kg) and xylazine (5 mg/kg) mixture, 10 min before the MRI imaging. The rats were then injected with the IUdR-loaded NGO/SPION/PLGA suspension (2 mg Fe/ kg) through the lateral tail vein and maintained in the EMF for 1 h. To determine magnetic nanoparticle distribution in the rat brain, 20 axial and coronal sections of the brain were obtained with a T2-weighted turbo-spin-echo with the following parameters: TR = 2300 m s, NEX = 3;TE = 107 m s: matrix size = 256×256 ; $FOV = 47 \text{ mm} \times 47 \text{ mm}$; slice thickness = 1.5 mm and number of slices = 20. T2-weighted images were obtained prior to and at 1 h post injection for rats with or without an EMF. Also, MRI signal intensity was processed with ITK-SNAP 3.4 software.

2.10. Tumor volume inhibition and survival curves

To verify the treatment efficacy of the IUdR-loaded NGO/SPION/PLGA when combined with an EMF, 42 gliomas rat were randomly and equally divided into 6 treatment groups (7 rats in each group), on the 14th day of post-intracranial tumor implantation. The animals in the control group were treated with physiological buffer saline. The rats in the other 5 groups were administered free IUdR, NGO/SPION/PLGA (\pm MF) or IUdR-loaded NGO/SPION/PLGA (\pm MF), through the tail vein with a dose of 5 mg/kg IUdR. The rats were treated under an external magnetic field with a magnetic strength of 0.35–0.4 T on the tumor area for 1 h. On the 17th day of post-glioma implantation, 5 rats of each group were sacrificed randomly, and the brain tissue was collected and fixed by 4% formaldehyde solution 24 h; glioma tumors were completely severed, and the tumor volume was calculated using Eq. (5):

Tumor volume (mm³) =
$$\pi \times (a \times b \times c)/6$$
 (5

Where a, b and c represent width, height and thickness, respectively. a, b, and c values were measured by a digital Vernier caliper. The other 6 rats in each group were kept for monitoring their life span and analyzed by the Kaplan – Meier survival curves. Body weights were measured every day for the duration of the experiment.

2.11. Histology of brain tumors

Glioma tissues were harvested 17 days following the C6 glioma cells injection and immediately fixed in 10% buffered formalin, embedded in paraffin, and sectioned in 4-µm thickness slices. Sections were stained by hematoxylin and eosin (H&E) per standard clinical laboratory protocol. Under a light microscope (Olympus CK2; Olympus Optical Co., Japan), tumor histology was viewed and imaged.

2.12. Statistical analysis

The results of this study are expressed as mean values \pm standard error of the mean (SEM), with "n" representing the number of experiments. For statistical scrutiny, one-way analysis of variance (ANOVA) followed by Tukey's test as the post hoc analysis was performed using the SPSS statistical software version16. A value of p < 0.05 was considered to be statistically significant.

3. Results

3.1. Cell characteristics

Monolayer culture of the C6 rat glioblastoma cell line was done on tissue culture flasks. The population doubling time determined from the log-phase of growth curve was approximately 18.41 \pm 0.76 h.

3.2. Synthesis and characterization of the nanoparticles

The physicochemical features of the blank nanoparticles (NGO/ SPION/PLGA) and IUdR-loaded NGO/SPION/PLGA are summarized in Table 1. The hydrodynamic diameter and zeta potentials of NGO/ SPION/PLGA nanoparticles were 36.8 nm and -32.92 mV, respectively, while the diameter and zeta potentials of IUdR-loaded nanoparticle increased to 71.8 nm and -33.07 mV after loading with IUdR, respectively. The negative zeta potential of the nanoparticles supports its sufficient stability in the aqueous medium [29]. A sphere-like morphology of IUdR-loaded nanoparticles was obtained by TEM image as illustrated in Fig. 1A. The dry nanoparticle sizes of blank and drug loaded nanoparticles were calculated by TEM images to be 11.5 nm and 26.3 nm, respectively, which were smaller than those obtained by DLS (1 B). It is a well demonstrated fact that DLS measures the hydrodynamic diameter by dispersing nanoparticles in aqueous phase resulting in polymer shell dehydration, whereas TEM determine the size of dried samples-loaded onto the copper grids [30]. The drug loading content (DLC) and encapsulation efficiency (EE) of IUdR-loaded NGO/ SPION/PLGA were calculated 3.04 \pm 0.46%, and 91.2 \pm 1.74%,

Table 1 Physico-chemical properties of blank nanoparticles (NGO/SPION/PLGA) and IUdR-loaded NGO/SPION/PLGA (n = 3, mean \pm standard error).

Properties	NGO/SPIO/PLGA	IUdR/NGO/SPIO/PLGA
Hydrodynamic diameter (nm)	36.8	71.8
Polydispersity index (PdI)	0.14	0.173
Zeta potential (mV)	-32.92 ± 0.04	-33.07 ± 0.07
Drug loading (%)		3.04 ± 0.46
Encapsulation efficacy (%)		91.2 ± 1.74
Saturation magnetization (emu/g)	37.93	15.98

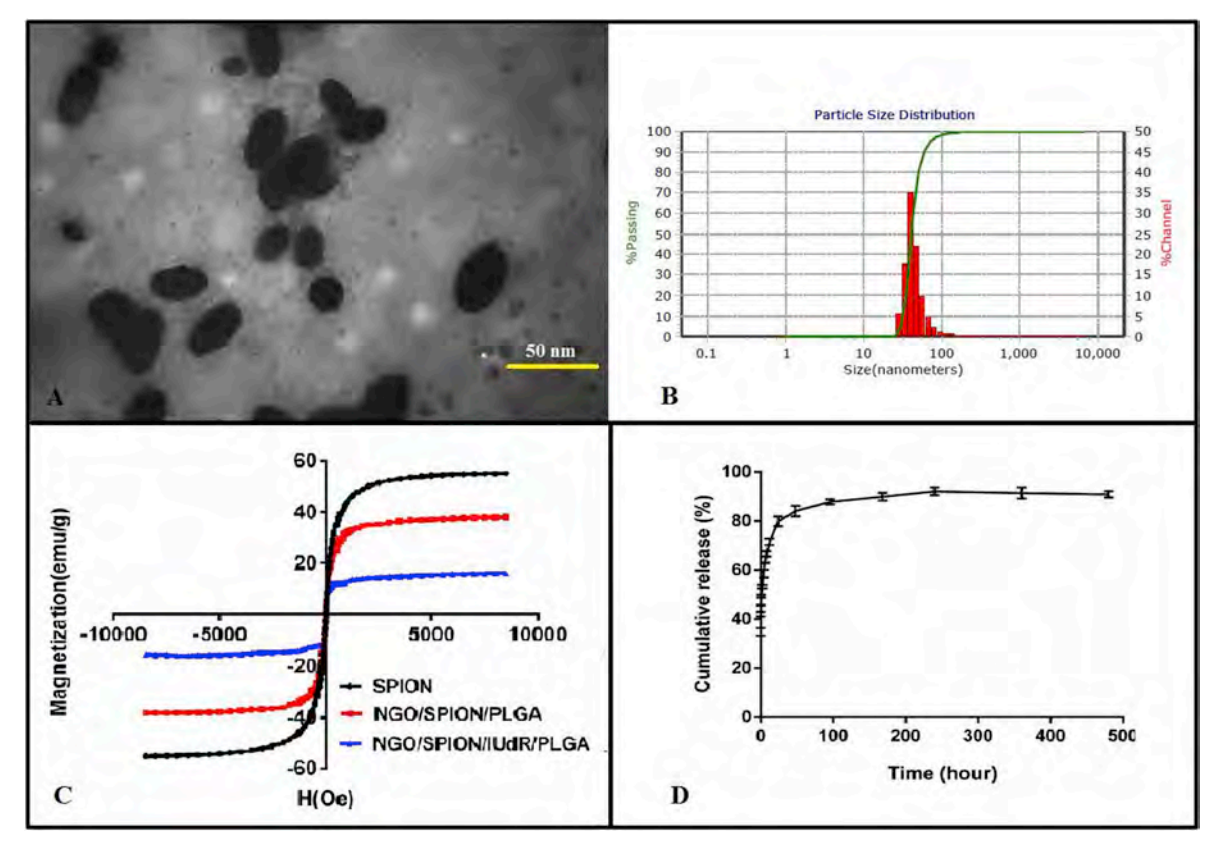


Fig. 1. (A) TEM images and (B) size distributions of the IUdR-loaded NGO/SPION/PLGA, (C) The room-temperature (25 °C) magnetic hysteresis curve of SPION, NGO/SPION/PLGA and IUdR/NGO/SPION/PLGA, (D) In vitro release profiles of IUdR from IUdR-loaded NGO/SPION/PLGA in PBS of pH 7.4 at 37 °C.

respectively. The variations of magnetization value under EMF for the samples are displayed in Fig. 1C. The magnetic hysteresis curves displayed that SPION, NGO/SPION/PLGA and IUdR-loaded nanoparticle were superparamagnetic with saturated magnetizations (Ms) of 55.14 emu/g, 37.93 emu/g and 15.98 emu/g, respectively. Reducing saturation magnetization of NGO/SPION/PLGA relative to blank could be due to the reduction in the magnetic interaction of SPION with diamagnetic PLGA-coated and graphene oxide sheets. Although the saturation magnetization of IUdR-loaded NGO/SPION/PLGA was lower than that of SPION and NGO/SPION/PLGA, the zero coercivity and no remanent magnetization of the IUdR-loaded NGO/SPION/PLGA suggested that the drug-loading process did not influence on the superparamagnetic behavior of the NGO/SPION/PLGA and could be easily attracted by magnet, as shown in Fig. 1C. This prevents MNPs from aggregation, and the nanoparticles can be dispersed rapidly when magnetic field is removed. Moreover, the magnetization property also affects the IUdR/ NGO/SPION/PLGA detection sensitivity of MRI.

3.3. In vitro drug release

The cumulative IUdR percentage of the nanoparticles at different time intervals in phosphate buffer (pH 7.4) at $37\,^{\circ}\mathrm{C}$ is shown in Fig. 1D. The IUdR-loaded NGO/SPION/PLGA showed a biphasic release curve consisting of a fast primary release followed by a sustained release, as in the first 8 h, the release was 67% and in the 24 h it was 79%. More than 85% of the drug was released within 48 h. The in vitro release of IUdR from the nanoparticle was monitored for a few days but release never reached 100%.

3.4. Photothermal effects of magnetic nanoparticles

The temperature increase of the cell culture medium induced by the alternative magnetic field (40 kA/m) is indicated in Fig. 2. Temperature

measurement during AMF exposure for MNPs samples within 10 min revealed a noticeable elevation from 25 to 65 °C, while the blank media (as control) displayed no obvious temperature change ($\Delta T = 11$ °C). According to Fig. 2, a significant difference was observed between the presence and absence of magnetic nanoparticles in RF hyperthermia at 13.56 MHz (P < 0.001). This suggests that magnetic nanoparticles under the AMF exposure could act as an effective photothermal agent.

3.5. In vitro cytotoxicity of IUdR-loaded NGO/SPION/PLGA

Cytotoxicity of the NPs on the growth of C6 glioma cells was evaluated using MTT assay. As shown in Fig. 3, the cell viability after treatment with NGO/SPION/PLGA remained over 70% even at the highest concentration (0.6 mg/mL) at 24 h, while, uncoated NGO nanoparticles are significantly more toxic than the coated NGO/SPION (p < 0.05, Fig. 3D). Therefore, as the results indicated, PLGA polymer coating of magnetic NGO nanoparticles increased their biocompatibility.

Also the figure shows the cytotoxicity profile of C6 glioma cells incubated with IUdR-loaded NGO/SPION/PLGA and free IUdR solution in various concentrations of IUdR. The cytotoxicity of IUdR/NGO/SPION/PLGA and IUdR were concentration dependent, and their inhibitory concentration (IC50) values were 42.18 \pm 0.21 and 160.3 \pm 0.96 µg/mL, respectively. Clearly, IUdR/NGO/SPION/PLGA exhibits a 3.8-fold intensification of C6 cell inhibition compared to free IUdR (p < 0.05, Fig. 3D). These results revealed that, when C6 glioma cells treated with an equivalent concentration of IUdR, they showed lower viability in treatment with IUdR-loaded nanoparticle than with free IUdR. This indicated that the NGO/SPION/PLGA have promising applications as intelligent drug delivery platform.

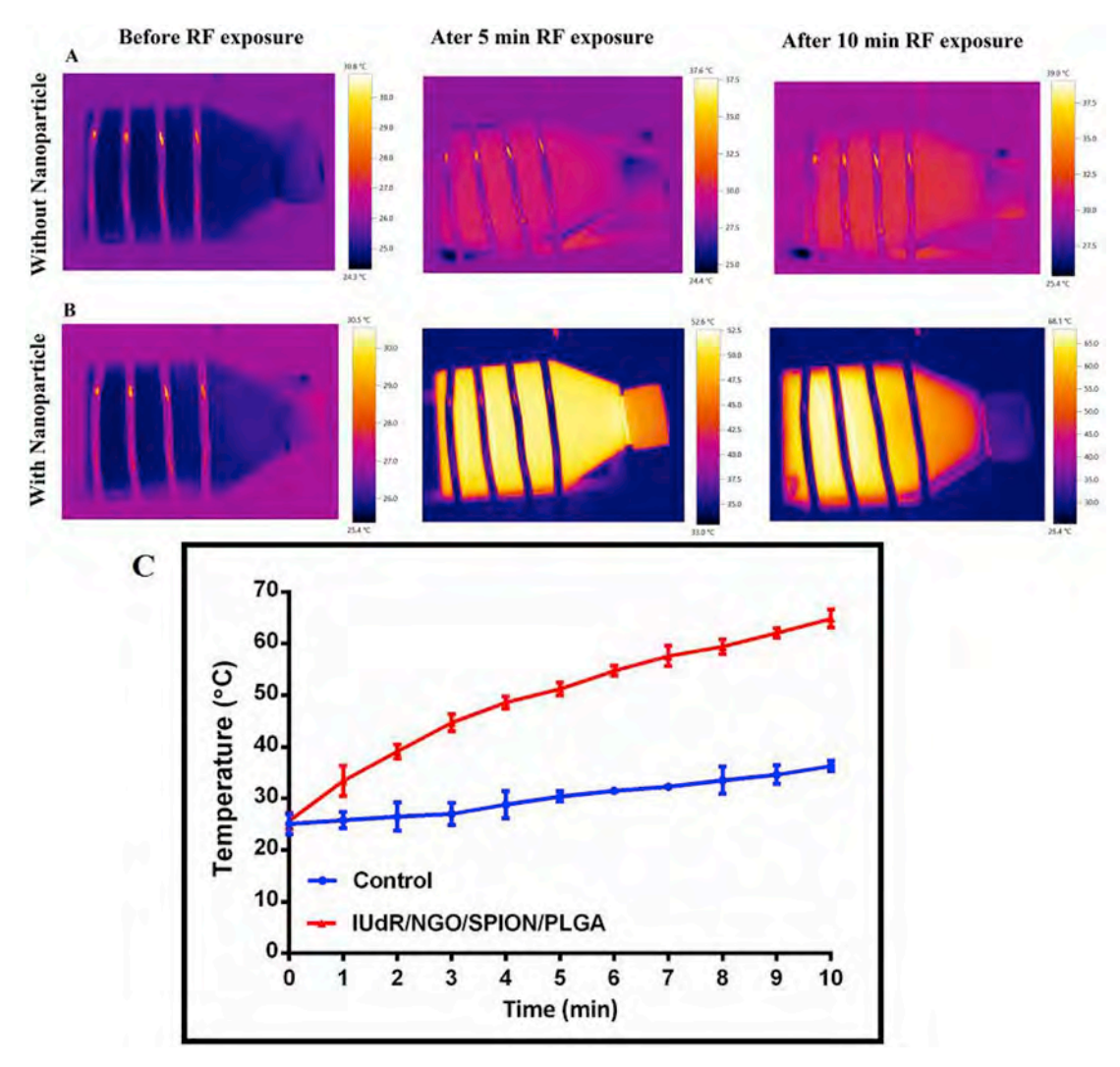


Fig. 2. Photothermal capacities of magnetic nanoparticle upon alternative magnetic field exposure with RF coil (40 kA/m, 13.56 MHz) for 10 min in (A) control and (B) with 1 mg/mL IUdR/NGO/SPION/PLGA in cell culture medium. The image shows the near-infrared images of the cell culture with and without nanoparticle in different exposure time, (C) Temperature–time curve AMF exposure. The data represent the mean \pm SD, n = 3 for three independent replicates.

3.6. In vivo magnetic targeting using the modified magnet configuration

The optimized magnet configurations, with their magnetic flux density mapping are presented in Fig. 4A. The goal of this design was to select a configuration that would produce a narrow area of maximum magnetic flux density and minimum the flux in the surrounding regions. As, the flux density value was found to decrease rapidly with increasing the longitudinal distance from the glioma location (Fig. 4B). Accordingly, while the measured flux density at the glioma site was 454 mT, the value measured 2.5 cm caudal to the tumor was 328 mT, indicating that the tumor would be exposed to a relatively maximum magnetic force, that it could be responsible for the nanoparticle accumulation in this area.

3.7. Brain glioma targeting of IUdR-loaded NGO/SPION/PLGA nanoparticles

To evaluate the magnetic field targeting effect in vivo and confirm whether NGO/SPION/PLGA nanoparticles could enhance the contrast of tumor imaging in rats, MRI T2-weighted images of rat brains were obtained before and 1 h post intravenous injection of magnetic nanoparticles in the axial and coronal directions. The MRI images of the gliomas are presented in Fig. 5A and B. The tumor was characterized by high intensity signals in the T2-weighted images before the injection of

NGO/SPION/PLGA. After the injection of magnetic nanoparticles, the most significant change in contrast was observed in rat glioma sites. Tumor areas darkening was distinct in post-injection of magnetic nanoparticle, indicating the enhanced negative contrast of NGO/SPION/ PLGA. Furthermore, the negative contrast improvement, in the applied of an EMF was more significant than without it, indicating that EMFs improved accumulation and retention of the NGO/SPION/PLGA to glioma. To prove the correlation of MRI contrast enhancement with targeted magnetic nanoparticle in animals, tumor tissue slices were stained with Prussian blue. Prussian blue staining is a typical method used to label Fe³⁺ in tissue samples as dark blue spots [30]. As shown in Fig. 5C and D, only a few blue spots were detected in rats administered with IUdR/NGO/SPION/PLGA and more nanoparticles were detected in rats administered with IUdR/NGO/SPION/PLGA in the presence of EMF. These results indicated NGO/SPION/PLGA nanoparticles could overcome the BBB for glioma targeting in the presence of an external magnetic field and could be used in noninvasive MR imaging techniques and enhance the MRI sensitivity to offer better chemotherapy and real time monitoring. Furthermore, Fig. 6 shows the changes in the signal intensity of MR imaging in tumor areas, tumors with nanoparticle accumulation and healthy tissue. Due to the high cell density of the tumor area, its signal intensity is higher than the healthy tissue, and because of the negative contrast of the SPIONs, the signal intensity of tumor containing the nanoparticles was lower than the

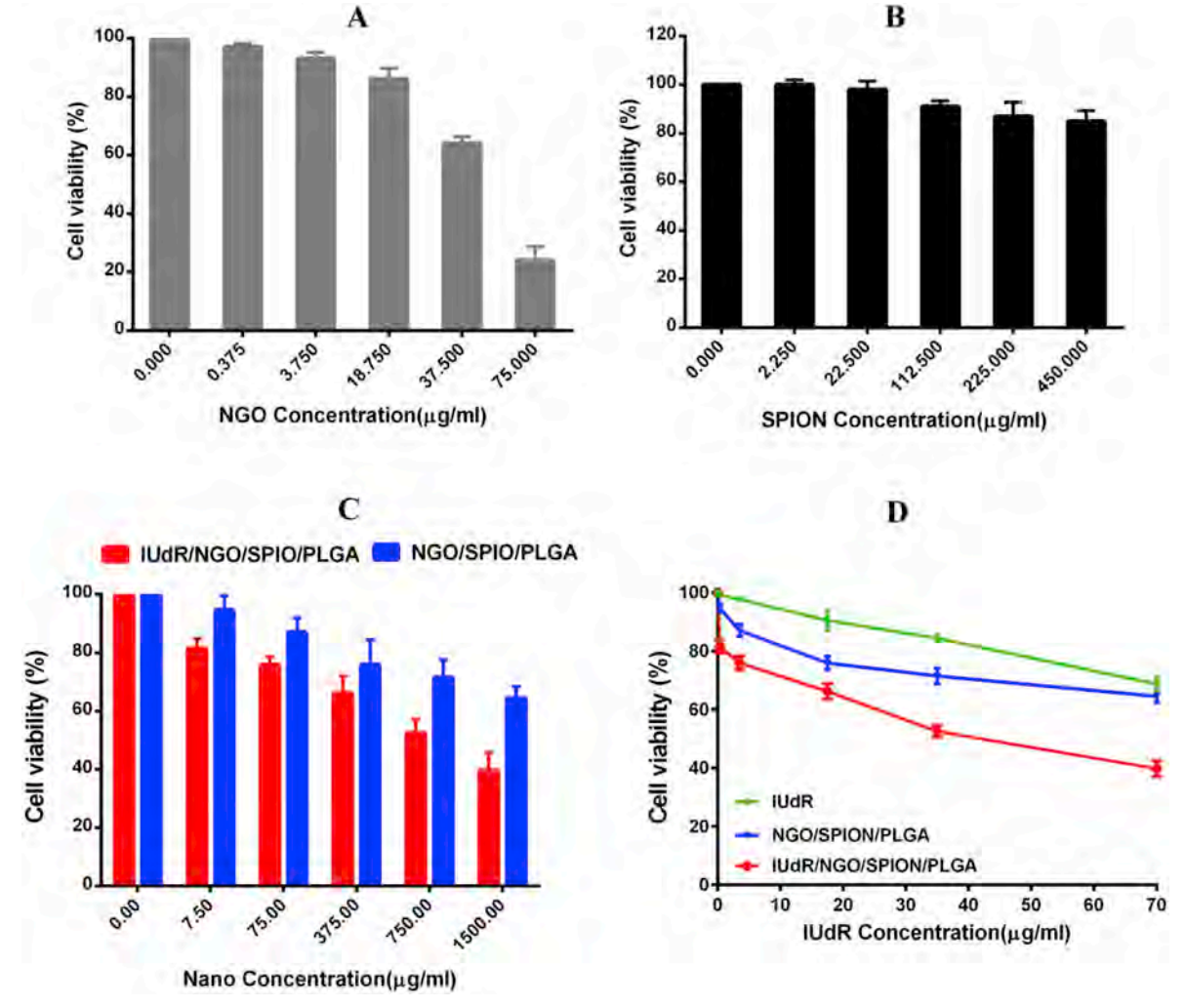


Fig. 3. Cell viability using MTT assay for C6 cells treated with different concentrations of (A) NGO, (B) SPION, (C) NGO/SPION/PLGA and IUdR/NGO/SPION/PLGA and (D) C6 viability – concentration curves for all concentrations of IUdR, MNPs and IUdR-loaded MNPs compared to each other. The results are expressed as the mean \pm standard deviation of three independent experiments.

other regions.

3.8. Tumor volume inhibition

To evaluate the antitumor effects of IUdR/MNPs on glioma-bearing rats, tumor volume was determined with MRI imaging (Fig. 7A).

After treatment with buffer saline, free IUdR, NGO/SPION/PLGA, NGO/SPION/PLGA + MF, IUdR/NGO/SPION/PLGA and IUdR/NGO/ SPION/PLGA + MF, tumor volume at the 17th day of post-intracranial implantation was 232.516, 207.28, 219.66, 209.78, 194.26 and 171.62 mm³, respectively (Fig. 6A). Post hoc analysis confirmed that IUdR/NGO/SPION/PLGA at the present magnetic field indicated the maximum inhibitory effect on tumor growth compared to other treatment groups (p < 0.01, Fig. 6A). Moreover, we evaluated the survival time of gliomas rat. After treatment with physiological saline, free IUdR, NGO/SPION/PLGA, NGO/SPION/PLGA + MF, IUdR/NGO/ SPION/PLGA and IUdR/NGO/SPION/PLGA + MF the survival range was 15-19, 17-28, 15-21, 17-23, 17-33, 24-42 days, respectively (Fig. 6 B). The rank of average survival time was IUdR/NGO/SPION/ PLGA + MF (38 days) > IUdR/NGO/SPION/PLGA (26.5 days) > IUdR (22.5 days) > NGO/SPION/PLGA + MF (19 days) > NGO/ SPION/PLGA (17.5 days) > saline (16.5 days). By the log-rank test, the average survival time of IUdR/NGO/SPION/PLGA under magnetic field was significantly increased compared with of the saline, IUdR, or

other groups (p < 0.01, Fig. 6B). The results indicated that in the rats treated with IUdR/NGO/SPION/PLGA together with MF, nanoparticles could further be transferred to the tumor site that was demonstrated using the MRI and Prussian blue staining. In fact, the combination of magnetic targeting and Nano-drug treatment exhibited promising anticancer effect compared to other groups as evidenced by the delay of tumor volume expansion.

3.9. Histology of brain tumors

The histological changes of rat brain tumors after treatments were detected by H&E staining. HE staining was performed by the paraffinembedded glioma tissues (Fig. 7). The H&E-stained sections from the saline group (control), free IUdR solution group, and IUdR/NGO/SPION/PLGA group were hypercellular and exhibited obvious huge cell nuclei, reflecting that the tumor from these groups had vigorous proliferative capability (Fig. 7B). On the contrary, tumor tissues from the IUdR/NGO/SPION/PLGA + MF group were hypocellular and showed the highest level of cell damage and extensive holes, indicating the highest anticancer effects (Fig. 7B).

4. Discussion

There are challenges impeding the brain tumor therapy, namely

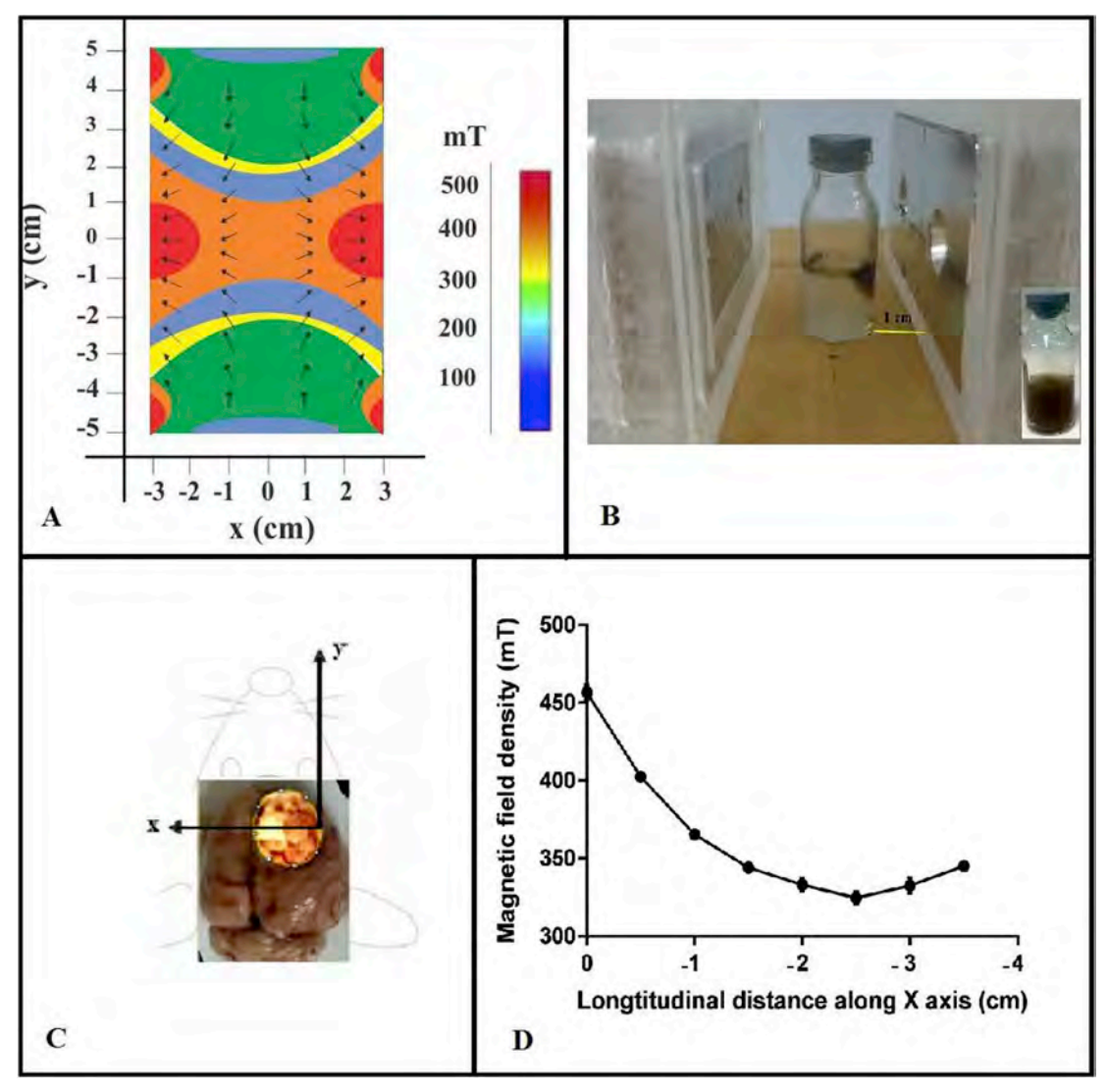


Fig. 4. Magnetic flux topography of the optimized magnet field between two permanent magnet NdFeB (1.3 T): (A) display magnetic flux maps measured with teslameter for the original magnetic field configurations, along the targeting plane, (B) Localization of IUdR/NGO/SPION/PLGA near magnet after 2 min, (C) Schematic diagram of the coordinate system with regard to the rat head used for magnetic flux density planning at the glioma zone, (D) Magnetic flux density curve measured along the X axes in direction with the EMF.

how to enhance the local accumulation and residence time of the chemotherapeutic drugs at the tumor mass, while avoiding accumulation in non-target organs. However, target selectivity is a critical factor in the design of Nano drug delivery systems for the noninvasive diagnoses and treatment of gliomas [4]. Recently, many researchers have focused on superparamagnetic nanoparticles for targeting drug delivery to brain and contrast enhancers to improve the sensitivity of MR imaging [31,32]. A major goal of the present investigation was to design and prepare NGO-based multifunctional magnetic PLGA-coated nanoparticles to cross the BBB, and targeted drug delivery of the anti-cancer drug IUdR to GBM under the regulation of an EMF. IUdR belongs to the group of antimetabolites and is highly hydrophilic (IUdR: 2 mg/ml), thus its distribution in a lipophilic brain tissue is low. Furthermore, for the halogenated pyrimidines the sensitization of the gliomas to radiation is proportional to the percentage of thymidine replacement in the replicating DNA, the high local concentration, and duration of exposure. After intravenous injection, however, the clearance of IUdR from the blood is rapid, toxicity is high, and the BBB may limit delivery [33,34]. To overcome these limitations, we showed that IUdR could be encapsulated in the magnetic NGO/PLGA nanoparticles. GO exhibited enhanced drug loading capacity, stability in different media and tumor

retention in vivo [35], however, NGO aggregation is easy due to its hydrophobic and electronic surface properties. PLGA contain of two polymers (PLA and PGA). PLA is hydrophobic and PGA is hydrophilic. A hydrophilic chains of PGA could increase the stability of nanocarrier in biological media and facilitate long blood circulation [36]. Also, for these radiosensitizers, local delivery is the most important parameter to amplify the effect of the radiotherapy on the brain tumors [37]. Thus, in order to create a vehicle capable of IUdR targeting to rat brain and MRI contrast agent, we utilized SPIONs. The use of SPIONs for in vivo applications must be modified with a biodegradable and nontoxic polymer to prevent the aggregation and improve stability and blood circulation times [38]. Thus, the nanoparticles suspensions prepared were truly superparamagnetic, and showed no evidence of aggregation (Fig. 1C). However, it should be noted that, the magnetization of SPIONs declines with decreasing the particle size [39]. Also, DLS results (Table 1) showed that these nanoparticles had an average diameter of \sim 72 nm, which enables efficient uptake using rat brain endothelial cells. The size of the nanoparticles is a key parameter in order to overcome difficulties involved in their transport across the endothelial barrier. According to the studies, Liu et al. (2013) and Zheng et al. (2016) the gaps between adjacent endothelial cells at tumor sites were 200 nm, even up to

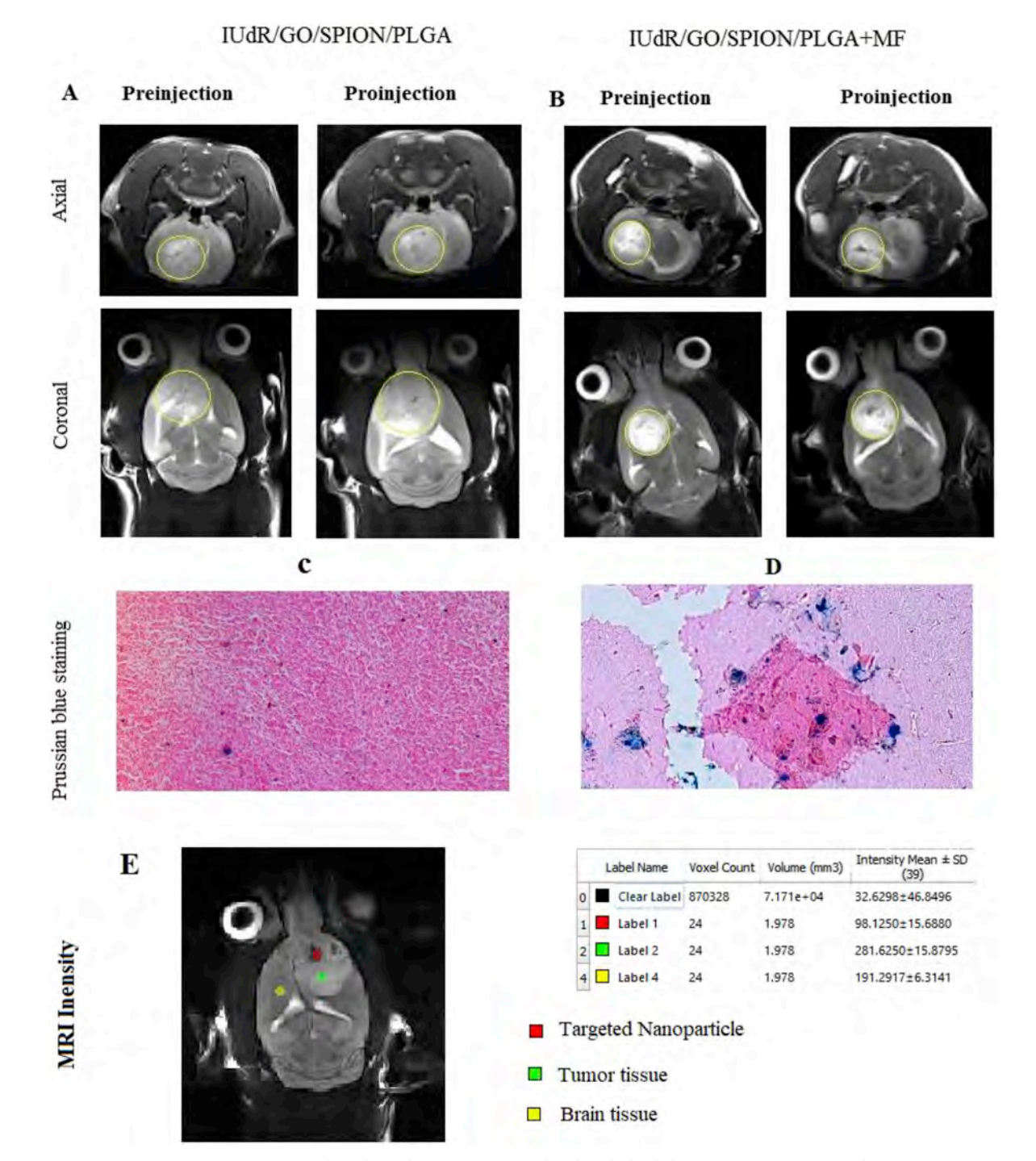


Fig. 5. Representative magnetic resonance images of C6 glioma bearing rats injected with IUdR-loaded NGO/SPION/PLGA (9 mg/kg). (A) MRI images were taken prior to and at 1 h post-administration of IUdR/NGO/SPION/PLGA alone and (B) with external magnetic field. Yellow dash circle represents the location of the glioma malignancy. The accumulation of magnetic nanoparticles appears as dark areas at the T2-weighted (Axial and Coronal) regimen. (C) the cryosections of rat brain with 4- μm thickness were stained with Prussian blue after administration of IUdR/NGO/SPION/PLGA alone and (D) with external magnetic field, (E) Intensity changes of MRI images for the three region, the tumor (green), tumor with nanoparticle (red) and normal brain tissue (yellow) of the same volume. (For interpretation of the references to color in this figure legend, the reader is referred to the Web version of this article.)

0.38 µm [13,40] and Jia et al. (2012) displayed that nanoparticles ranging from 10 to 100 nm in diameter were optimal for systemic administration, could cross the BBB and demonstrated the most increased blood circulation times [33]. IUdR loaded in magnetic nanoparticles displayed stronger inhibition of C6 cell proliferation than free IUdR (Fig. 3), which was similar to results reported by Ge'ze et al. (1999) [41]. The results demonstrate that cytotoxicity of IUdR/NGO/SPION/PLGA increases with increasing nanoparticle concentrations from 0.3 to

70 µg/mL that was also verified by other studies [11,42]. Cytotoxicity of NGO/SPION/PLGA was evaluated (Fig. 3), no significant toxicity was found at the highest concentration (0.6 mg/mL), and the cellular viability was above 70%, this findings was similar to results reported by Liu et al. (2013) [13]. To assess whether the designed IUdR/NGO/SPION/PLGA could be delivered to glioma sites by an EMF, the nanoparticles tracking were evaluated using Prussian blue staining and MR imaging. The magnetic field source applied in the present study was

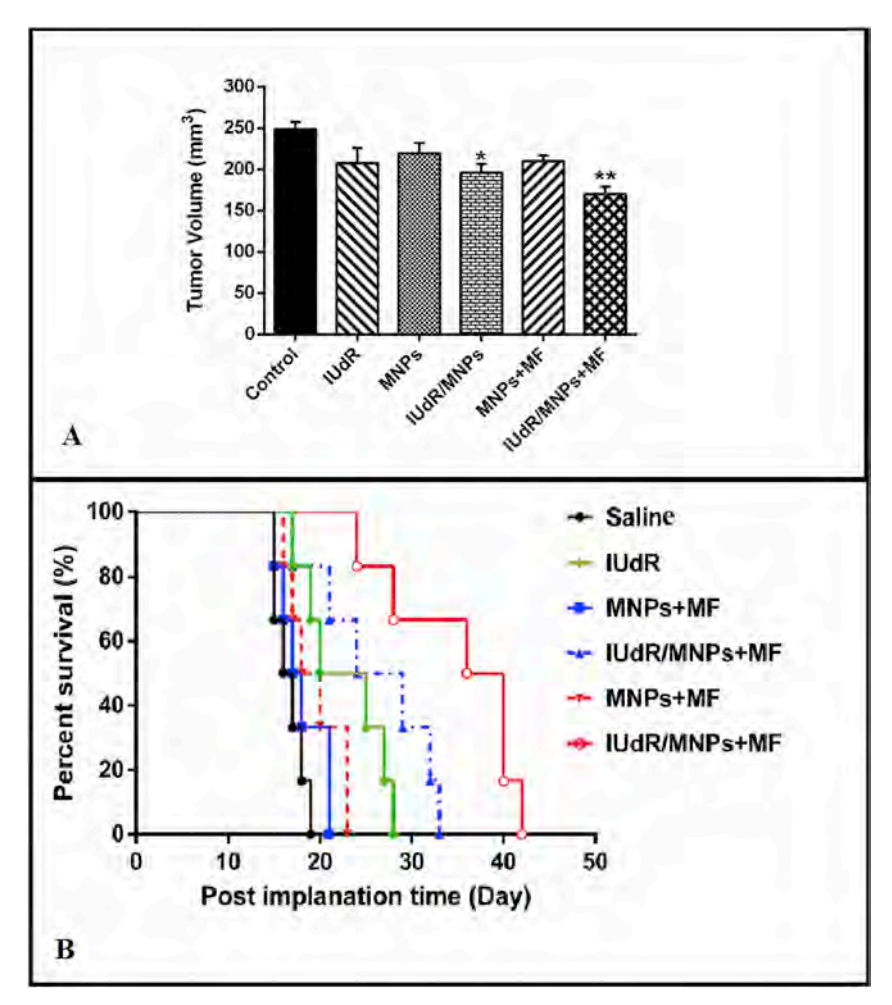


Fig. 6. Anti-glioma effects of IUdR/NGO/SPION/PLGA + MF vs IUdR/NGO/SPION/PLGA, NGO/SPION/PLGA + MF, NGO/SPION/PLGA, free IUdR, or control group after i. v. of 5 mg/kg IUdR on 14th day of post-intracranial implantation. (A) glioma tumor volume in different treatment groups on the 17th day, p < 0.01 (n = 3), (B) percentage of survival (Kaplan – Meier plot) (mean \pm SD, n = 6).

optimized to create a sharp gradient magnetic force to avoid the aggregation of non-specific IUdR-loaded magnetic nanoparticles away from the gliomas site (Fig. 4D). The results indicated that in the direction of a magnetic field, more blue spots were observed in the brain tissue slice (Fig. 5D). It may be because of the fast decay of the magnetic force with increasing the distance from the tumor area. Accumulation of nanoparticles to a specific region of the rat body could be regulated

by changing their exposure to the applied EMF and the shape and size of the magnet, for minimizing the toxicity. Our findings were in agreement to the results reported by Chertok et al. (2008) and Xu et al. (2016) and Hua et al. (2011) [4,5,30]. Therefore, an additional goal of the present research was to develop a MRI technique for non-invasive monitoring of SPIONs brain tumor [21,43]. SPIONs as negative contrast agents enhance MRI sensitivity due to a reduced T2 relaxation time. In

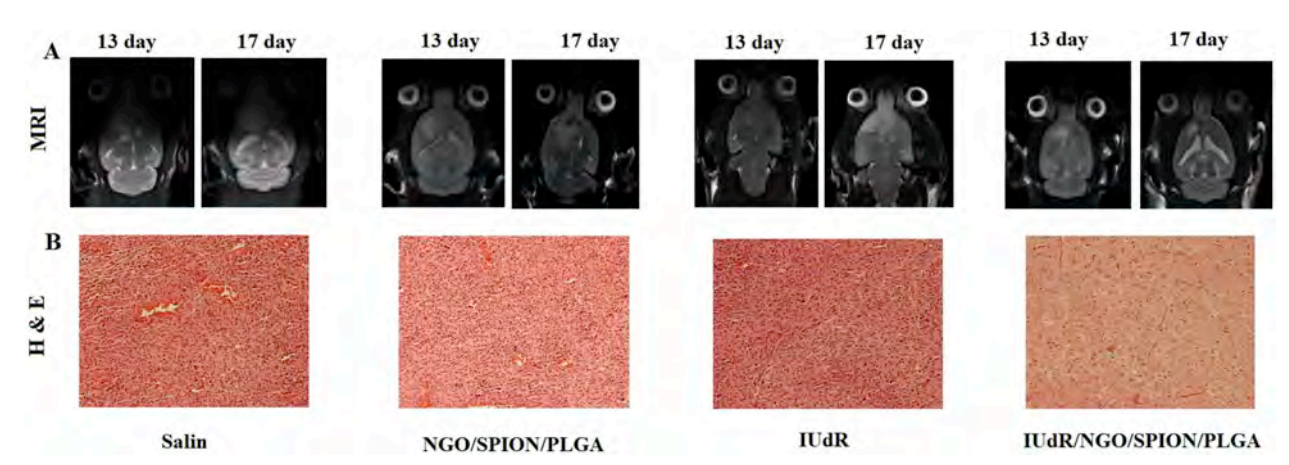


Fig. 7. (A) Coronal T2-weighted images of C6 glioma bearing rats obtained for treatment groups at the different time points (preradiation and at 17 days' post injection). (B) Sections (thickness of $4 \mu m$) of C6 glioma from control group vs IUdR, NGO/SPION/PLGA + MF and IUdR/NGO/SPION/PLGA + MF excised on the 17th day (three days after treatment) were evaluated by microscopy after stained with hematoxylin and eosin for histopathological analysis.

this study, the MRI imaging contrast enhancement of rat glioma tumor in axial and coronal sections was confirmed by i. v. injections of IUdR/ NGO/SPION/PLGA nanoparticles (Fig. 5A and B). The results showed that NGO/SPION/PLGA nanoparticles could be used as potential contrast agents for tumor malignant detection. Another interesting application of SPIONs is the production of heat under the influence of the alternative magnetic field [44]. The results indicated that, due to the thermally activated switching of the magnetic moment of MNPs under alternative magnetic field, IUdR/NGO/SPION/PLGA may offer remarkably improved photothermal efficacy under RF hyperthermia as the excitation source (Fig. 2). Applying an external alternative magnetic field operating at a specific frequency causes the magnetic nanoparticles to heat by hysteresis loss. Neel relaxation, and induced eddy currents [45]. Furthermore, Yu et al. (2014) showed that, when magnetic NPs were subjected to an external radiofrequency source (50 kHz), the release rate of drugs increased and then decreased when the RF source was off [46]. In the following, the antitumor efficacy of IUdRloaded nanoparticles in C6 glioma-bearing rats was assessed by tumor volume. Our results showed that rats treated with IUdR/NGO/SPION/ PLGA in combination with designed magnetic field exhibited the strongest inhibitory effect and longer survival times on tumor growth compared to the other treated groups (Fig. 6A and B) [13,47]. Nanoparticle toxicity and histological changes of rat gliomas after different treatment modalities were detected by HE staining. Finally, these data demonstrated that IUdR/NGO/SPION/PLGA multifunctional nanoparticle under external magnetic field display the strongest antitumor effect in rat gliomas, indicating that targeted NGO/SPION/PLGA may be a suitable platform for the transport of IUdR across BBB, decreased total chemotherapeutic drug dose to lower the toxicity of drugs circulating in the blood and MRI contrast agent.

5. Conclusion

Advances in multifunctional nanoparticles based diagnostic and therapeutic platforms are expected to provide enormous potential for the enhancement of diagnosis and treatment methods of cancers. In the present study, for the first time, we have combined the concepts from two fields to synthesize IUdR-loaded magnetic nanoparticles and indicated its high-level specificity to magnetic targeting C6 glioma cells both in vitro and in vivo as well as its ability to act as an excellent contrast enhancement agent for MRI. In comparison studies with control nanoparticle (NGO/SPION/PLGA), we showed a profound difference between non-targeting and targeting external magnetic field in tumor accumulation, which may be attributed to the prolonged retention in tumors sites. This innovation increases the possibility of improving clinical therapeutic efficiency of chemotherapy agents, or lowering the total anticancer-drug dose to decrees systemic toxicity.

Declaration of interest

The authors report no conflicts of interest. The authors alone are responsible for the content and writing of the paper.

Acknowledgements

This research was supported by grant No. 26884 from the School of Medicine, Iran University of Medical Sciences (IUMS), Tehran, IRAN.

Appendix A. Supplementary data

Supplementary data related to this article can be found at https://doi.org/10.1016/j.cbi.2018.08.027.

Transparency document

Transparency document related to this article can be found online at

https://doi.org/10.1016/j.cbi.2018.08.027.

References

- B. Chertok, A.E. David, V.C. Yang, Polyethyleneimine-modified iron oxide nanoparticles for brain tumor drug delivery using magnetic targeting and intra-carotid administration, Biomaterials 31 (24) (2010) 6317–6324.
- [2] A. Jain, et al., Guiding intracortical brain tumour cells to an extracortical cytotoxic hydrogel using aligned polymeric nanofibres, Nat. Mater. 13 (3) (2014) 308–316.
- [3] J.K. Saucier-Sawyer, et al., Distribution of polymer nanoparticles by convectionenhanced delivery to brain tumors, J. Contr. Release 232 (2016) 103–112.
- [4] B. Chertok, et al., Iron oxide nanoparticles as a drug delivery vehicle for MRI monitored magnetic targeting of brain tumors, Biomaterials 29 (4) (2008) 487–496.
- [5] H.-L. Xu, et al., Glioma-targeted superparamagnetic iron oxide nanoparticles as drug-carrying vehicles for theranostic effects, Nanoscale 8 (29) (2016) 14222–14236.
- [6] H. Liu, et al., Application of iron oxide nanoparticles in glioma imaging and therapy: from bench to bedside, Nanoscale 8 (15) (2016) 7808–7826.
- [7] M. Tamborini, et al., A combined approach employing chlorotoxin-nanovectors and low dose radiation to reach infiltrating tumor niches in glioblastoma, ACS Nano 10 (2) (2016) 2509–2520.
- [8] B. Sahoo, et al., Thermal and pH responsive polymer-tethered multifunctional magnetic nanoparticles for targeted delivery of anticancer drug, ACS Appl. Mater. Interfaces 5 (9) (2013) 3884–3893.
- [9] A. Singh, S.K. Sahoo, Magnetic nanoparticles: a novel platform for cancer theranostics, Drug Discov. Today 19 (4) (2014) 474–481.
- [10] L. Han, et al., Increased nanoparticle delivery to brain tumors by autocatalytic priming for improved treatment and imaging, ACS Nano 10 (4) (2016) 4209–4218.
- [11] Y. Yu, et al., Antitumor activity of doxorubicin-loaded carbon nanotubes incorporated poly (lactic-co-glycolic acid) electrospun composite nanofibers, Nanoscale research letters 10 (1) (2015) 343.
- [12] H. Wu, et al., Hyaluronic acid conjugated graphene oxide for targeted drug delivery, Carbon 69 (2014) 379–389.
- [13] G. Liu, et al., Transferrin modified graphene oxide for glioma-targeted drug delivery: in vitro and in vivo evaluations, ACS Appl. Mater. Interfaces 5 (15) (2013) 6909-6914
- [14] A. Sahu, et al., Graphene oxide mediated delivery of methylene blue for combined photodynamic and photothermal therapy, Biomaterials 34 (26) (2013) 6239–6248.
- [15] N. Ardjomandi, et al., Coating of ß-tricalcium phosphate scaffolds—a comparison between graphene oxide and poly-lactic-co-glycolic acid, Biomed. Mater. 10 (4) (2015) 045018
- [16] Y.-J. Lu, et al., Improving thermal stability and efficacy of BCNU in treating glioma cells using PAA-functionalized graphene oxide, Int. J. Nanomed. 7 (2012) 1737–1747
- [17] S. Kargar, et al., Evaluation of the combined effect of NIR laser and ionizing radiation on cellular damages induced by IUdR-loaded PLGA-coated Nano-graphene oxide, Photodiagn. Photodyn. Ther. 21 (2018) 91–97.
- [18] S. Khoei, et al., Effects of resveratrol and methoxyamine on the radiosensitivity of iododeoxyuridine in U87MG glioblastoma cell line, Exp. Biol. Med. 241 (11) (2016) 1229–1236.
- [19] L.I. Wiebe, et al., Preparation and preliminary evaluation of novel β -cyclodextrin/IUDR prodrug formulations, J. Pharm. Pharmaceut. Sci. 11 (2) (2008) 32–43s.
- [20] U.O. Häfeli, et al., Cell uptake and in vitro toxicity of magnetic nanoparticles suitable for drug delivery, Mol. Pharm. 6 (5) (2009) 1417–1428.
- [21] M.A. Shevtsov, et al., Tumor targeting using magnetic nanoparticle Hsp70 conjugate in a model of C6 glioma, Neuro Oncol. 16 (1) (2014) 38–49.
- [22] M. Liong, et al., Multifunctional inorganic nanoparticles for imaging, targeting, and drug delivery, ACS Nano 2 (5) (2008) 889.
- [23] C.-H. Fan, et al., SPIO-conjugated, doxorubicin-loaded microbubbles for concurrent MRI and focused-ultrasound enhanced brain-tumor drug delivery, Biomaterials 34 (14) (2013) 3706–3715.
- [24] S. Khoee, A. Kavand, Preparation, co-assembling and interfacial crosslinking of photocurable and folate-conjugated amphiphilic block copolymers for controlled and targeted drug delivery: smart armored nanocarriers, Eur. J. Med. Chem. 73 (2014) 18–29.
- [25] D.C. Marcano, et al., Improved synthesis of graphene oxide, ACS Nano 4 (8) (2010) 4806–4814.
- [26] M. Ashjari, S. Khoee, A.R. Mahdavian, A multiple emulsion method for loading 5-fluorouracil into a magnetite-loaded nanocapsule: a physicochemical investigation, Polym. Int. 61 (5) (2012) 850–859.
- [27] M. Zhao, et al., Magnetic paclitaxel nanoparticles inhibit glioma growth and improve the survival of rats bearing glioma xenografts, Anticancer Res. 30 (6) (2010) 2217–2223.
- [28] B. Chertok, A.E. David, V.C. Yang, Brain tumor targeting of magnetic nanoparticles for potential drug delivery: effect of administration route and magnetic field topography, J. Contr. Release 155 (3) (2011) 393–399.
- [29] F. Dilnawaz, et al., Dual drug loaded superparamagnetic iron oxide nanoparticles for targeted cancer therapy, Biomaterials 31 (13) (2010) 3694–3706.
- [30] M.-Y. Hua, et al., Superhigh-magnetization nanocarrier as a doxorubicin delivery platform for magnetic targeting therapy, Biomaterials 32 (34) (2011) 8999–9010.
- [31] S. Valable, et al., In vivo MRI tracking of exogenous monocytes/macrophages targeting brain tumors in a rat model of glioma, Neuroimage 37 (2007) S47–S58.
- [32] P.-Y. Chen, et al., Novel Magnetic/ultrasound Focusing System Enhances Nanoparticle Drug Delivery for Glioma Treatment, Neuro-oncology, 2010, p. noq054.

- [33] Y. Jia, et al., Co-encapsulation of magnetic Fe3O4 nanoparticles and doxorubicin into biodegradable PLGA nanocarriers for intratumoral drug delivery, Int. J. Nanomed. 7 (2012) 1697.
- [34] T.W. Rösler, et al., Diesterified derivatives of 5-iodo-2'-deoxyuridine as cerebral tumor tracers, PLoS One 9 (7) (2014) e102397.
- [35] T.H. Tran, et al., Development of a graphene oxide nanocarrier for dual-drug chemo-phototherapy to overcome drug resistance in cancer, ACS Appl. Mater. Interfaces 7 (51) (2015) 28647-28655.
- W. Miao, et al., Cholesteryl hyaluronic acid-coated, reduced graphene oxide na-
- nosheets for anti-cancer drug delivery, Biomaterials 34 (37) (2013) 938–9647.

 [37] X. Yuan, et al., Synthetic, implantable, biodegradable polymers for controlled release of radiosensitizers, Cancer Biother. Radiopharm. 14 (3) (1999) 177-186.
- [38] C. Nazli, et al., RGDS-functionalized polyethylene glycol hydrogel-coated magnetic iron oxide nanoparticles enhance specific intracellular uptake by HeLa cells, Int. J. Nanomed. 7 (2012) 1903.
- [39] Y.-w. Jun, et al., Nanoscale size effect of magnetic nanocrystals and their utilization for cancer diagnosis via magnetic resonance imaging, J. Am. Chem. Soc. 127 (16) (2005) 5732-5733.
- [40] S. Zheng, et al., Biodegradable micelles enhance the antiglioma activity of curcumin

- in vitro and in vivo, Int. J. Nanomed. 11 (2016) 2721.
- [41] A. Géze, et al., Modulated release of IdUrd from poly (D, L-lactide-co-glycolide) microspheres by addition of poly (D, L-lactide) oligomers, J. Contr. Release 58 (3) (1999) 311-322.
- S. Jaworski, et al., In vitro evaluation of the effects of graphene platelets on glioblastoma multiforme cells, Int. J. Nanomed. 8 (1) (2013) 413-420.
- [43] N. Coquery, et al., Intrahippocampal transplantation of mesenchymal stromal cells promotes neuroplasticity, Cytotherapy 14 (9) (2012) 1041–1053.
- E.C. Abenojar, et al., Structural effects on the magnetic hyperthermia properties of iron oxide nanoparticles, Prog. Nat. Sci.: Materials International 26 (5) (2016)
- [45] R.A. Revia, M. Zhang, Magnetite nanoparticles for cancer diagnosis, treatment, and treatment monitoring: recent advances, Mater. Today 19 (3) (2016) 157-168.
- [46] L. Yu, et al., Evaluation of hyperthermia of magnetic nanoparticles by dehydrating DNA, Sci. Rep. 4 (2014) 7216.
- [47] T.J. Kinsella, et al., An in vivo comparison of oral 5-iodo-2'-deoxyuridine and 5iodo-2-pyrimidinone-2'-deoxyribose toxicity, pharmacokinetics, and DNA incorporation in athymic mouse tissues and the human colon cancer xenograft, HCT-116, Canc. Res. 54 (10) (1994) 2695-2700.